metals

MDPI

Article

Effect of Bismuth Content and Heating Rate on MnS Inclusions in Free-Cutting Steel

Chunlu Xie [1], Hongmei Zhang [1,2,*], Gang Zhao [2,*], Xiangyu Li [1], Hongnan Li [1], Guoao Yu [1] and Zhengyi Jiang [3,*]

[1] School of Materials and Metallurgy, University of Science and Technology Liaoning, Anshan 114051, China
[2] State Key Laboratory of Metal Material for Marine Equipment and Application, Anshan 114051, China
[3] School of Mechanical, Materials, Mechatronic and Biomedical Engineering, University of Wollongong, Wollongong 2522, NSW, Australia
* Correspondence: zhanghm@ustl.edu.cn (H.Z.); zg0476@126.com (G.Z.); jiang@uow.edu.au (Z.J.); Tel.: +86-138-0492-7151 (H.Z.); +86-188-1650-7540 (Z.J.)

Abstract: In this paper, the influence of bismuth content and heating rate on the morphology of MnS inclusions in bismuth-containing free-cutting steel during heating was investigated through in situ observation experiments and 3D electrolytic corrosion experiments. By observing the microscopic morphology of inclusions in the original sample, it was found that MnS inclusions in the sample were rod-shaped, spherical, irregular, small in size, and mostly clustered at the grain boundary in the form of chains and divergences. With the addition of bismuth, MnS inclusions of a larger size appear in the steel, and the inclusions distributed at grain boundaries are also reduced. When bismuth (0.010~0.020%) is added to the steel, MnS is mainly spherical and uniformly dispersed in the steel matrix. If the bismuth content is too high, the inclusions aggregate. Through in situ observations of the inclusions in the sample, it was found that the addition of bismuth in the heating process delays the appearance of ferrite grain boundaries and contributes to the spheroidization of MnS inclusions. Mn and S elements can fully diffuse slowly in the matrix with a heating rate below 1 °C/s and a long holding time (300 s), which provides the possibility for the spheroidization of MnS inclusions.

Keywords: free-cutting steel; bismuth; inclusion; 3D electrolytic corrosion; in situ observation

check for updates

Citation: Xie, C.; Zhang, H.; Zhao, G.; Li, X.; Li, H.; Yu, G.; Jiang, Z. Effect of Bismuth Content and Heating Rate on MnS Inclusions in Free-Cutting Steel. *Metals* **2024**, *14*, 713. https://doi.org/10.3390/met14060713

Academic Editor: Umberto Prisco

Received: 13 May 2024
Revised: 11 June 2024
Accepted: 12 June 2024
Published: 16 June 2024

Copyright: © 2024 by the authors. Licensee MDPI, Basel, Switzerland. This article is an open access article distributed under the terms and conditions of the Creative Commons Attribution (CC BY) license (https://creativecommons.org/licenses/by/4.0/).

1. Introduction

Free-cutting steel refers to steel that adds free-cutting elements, such as S, Pb, Bi, Te, etc., to conventional steel alone or mixed to improve its chip performance and thus obtain high processing accuracy, low processing costs, and good cutting performance [1–3]. Compared with ordinary steel, this kind of steel has the characteristics of easy chip breaking, a lower cutting resistance, lower energy consumption, and a longer tool life during processing [4].

Under the current trend of environmental protection, countries all over the world are advocating "green steel", and new steel grades that meet the requirements of environmental protection have been developed to ban the seriously polluting lead-series free-cutting steel [5–8]. In order to achieve this goal, researchers continue to explore new types of steel, among which bismuth and tellurium have become research hotspots to replace lead-based easy-cutting steel because of their similar properties to lead [9]. It has been found that the added bismuth content only needs half or less of the lead content to achieve a cutting performance comparable to that of lead-based easy-cutting steel [10]. By adding the right amount of bismuth, it is expected to achieve the balance between environmental protection and the machinability of free-cutting steel [11].

The cutting performance of free-cutting steel is determined by the size, morphology, and distribution of MnS inclusions [12]. Generally speaking, MnS inclusions with a small size and uniform distribution in the form of balls and spindles are the most favorable for the cutting performance of steel [13]. Therefore, effective control of the shape of MnS inclusions is the key to obtain high-quality free-cutting steel [5,14,15].

At present, high-temperature confocal laser microscopy has been widely used in the field of iron and steel materials; in order to further study the excellent cutting properties of free-cutting steel, high-temperature confocal microscopy has also been invested in the study of free-cutting steel. For example, Shen Chang et al. observed the precipitation of MnS inclusions in low-sulfur steel by using high-temperature confocal microscopy [16,17]. Shen et al. [18] observed the formation and growth behavior of Al_2O_3 inclusions in steel through high-temperature confocal microscopy and made a theoretical analysis of the observation results, providing a theoretical basis for further controlling the size distribution of inclusions in steel. Shao Xiaojing et al. used high-temperature confocal microscopy to observe in situ the dynamic evolution process of large-sized and long-strip MnS inclusions in high-sulfur free-cutting steel and non-tempered free-cutting steel [19,20].

The cutting performance of bismuth free-cutting steel is mainly closely related to the MnS inclusions in steel [21] and is significantly affected by the size, morphology, quantity, and distribution of inclusions [22–26]. At present, most of the research is mainly on sulfur-series free-cutting steel, and the analysis of inclusions in environmentally friendly free-cutting steel (such as bismuth-series free-cutting steel) is less prevalent. In this paper, the morphologies of MnS inclusions in bismuth-containing free-cutting steel during heating were dynamically observed in situ by using a high-temperature confocal laser microscope, and the effects of chemical composition, heating rate, and holding time on the morphology, distribution, and quantity of MnS in the steel were studied. The study of this subject can not only reveal the feasibility of substituting bismuth for lead, but also prove that the addition of bismuth is conducive to improving the morphology distribution and size number of inclusions [27,28] and the cutting performance.

2. Materials and Methods

2.1. Experimental Materials

The experimental material selected in this paper is bismuth-containing free-cutting steel, and the main chemical elements of the steel used are shown in Table 1.

Table 1. Chemical components of bismuth-containing free-cutting steel (mass fraction, %).

Sample	C	Si	Mn	P	S	Bi	Mn/S
1#	0.073	0.030	1.07	0.076	0.28	——	3.82
2#	0.064	0.035	0.90	0.081	0.28	0.010	3.21
3#	0.065	0.012	0.89	0.079	0.22	0.013	4.05
4#	0.068	0.031	1.06	0.081	0.31	0.022	3.42
5#	0.067	0.016	1.14	0.058	0.29	0.026	3.93
6#	0.072	0.032	1.08	0.078	0.31	0.031	3.48

2.2. Metallographic Experiment

In order to observe the microstructure and inclusion distribution of the test steel, the steel was first polished and corroded, and then observed and analyzed with a Keyens VHX-5000 metallographic microscope (KEYENCE Corporation, Osaka, Japan).

2.3. Three-Dimensional Electrolysis Characterization of Inclusions

Sample preparation. First, the test steel was made into a sample according to the size (16 × 8 × 4 mm), and its maximum surface was ground and polished. After polishing, the surface of the sample was cleaned with alcohol, and then, the remaining surface that was not ground and polished was wrapped with paraffin wax to prevent corrosion.

Electrolysis experiment. The treated sample was used as the positive electrode of the anode connected to the power supply, and the negative electrode was connected to the stainless steel sheet. In the electrolyte, the polishing surface and the stainless steel were validated, then the current and voltage were adjusted, and the test was started. The electrolytic time was about 2 h.

Sample cleaning and scanning electron microscope observations. After electrolytic corrosion, the material precipitated on the surface of the steel. After electrolytic corrosion, the 3 experimental steels needed to be cleaned with anhydrous ethanol. After cleaning, the surface of the samples was uneven, and the morphology of the inclusions in the samples was observed by scanning electron microscopy (ΣIGMA, Zeiss, Germany).

2.4. High-Temperature In Situ Observation Experiment

Sample preparation. First, the experimental steel was machined into a sample size of Φ7 × 2.5 mm and then polished.

Confocal experiment. The prepared sample was put into the alumina ceramic crucible and then into the high-temperature confocal laser microscope furnace, and the real-time dynamic observation of the experimental steel during the heating process could be carried out through the computer system connected with the high-temperature laser confocal microscope.

In order to study the effects of chemical composition, heating rate, and holding time on the inclusions in steel, different heating schemes have been developed, and the process parameters are shown in Table 2.

Table 2. Process parameters of high-temperature in situ observation experiment.

Sample	Heating Rate (°C/s)	Holding Time (s)	Holding Temperature (°C)	Cooling Rate (°C/s)
1#–6#	5	180	1250	2
	1			
4#	5	180	1250	2
	10			

3. Experimental Results and Discussion

3.1. Metallographic Observation of Nonmetallic Inclusions in Bismuth-Containing Free-Cutting Steel

Figure 1 shows the metallographic microstructure of six groups of experimental steels. It can be seen that the microstructure of the test steel is composed of pearlite, ferrite, and inclusions, in which the ferrite grain size is uneven. The 1# inclusions are mostly distributed in chains, clusters, and divergences within grains or along grain boundaries, as shown in Figure 1a. The inclusions of 2# and 3# are mostly dispersed in the steel matrix in the form of chains and scattered spots, as shown in Figure 1b,c. The inclusions of 4# are pearlite and mostly distributed in chains, clusters, and scattered spots inside the grains or at the grain boundaries, as shown in Figure 1d. The inclusions of 5# and 6# are mostly distributed in chains or clusters at grain boundaries, as shown in Figure 1e,f.

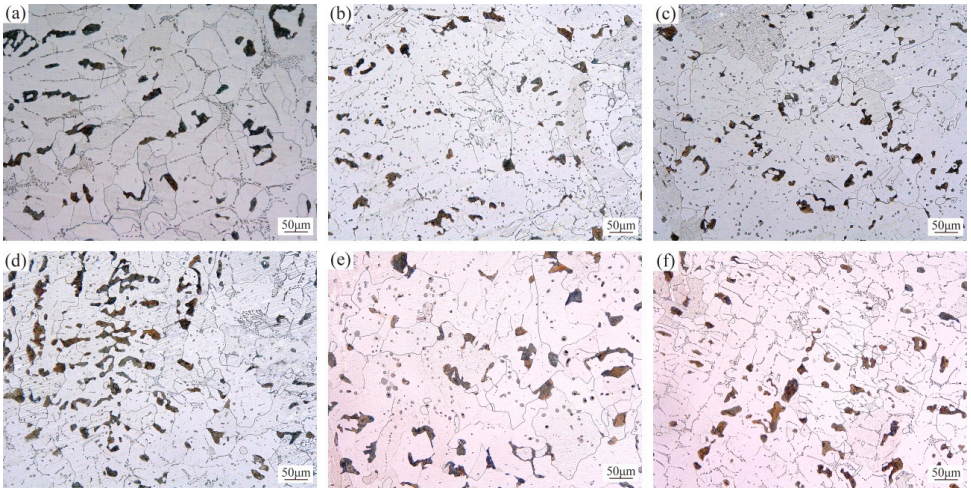


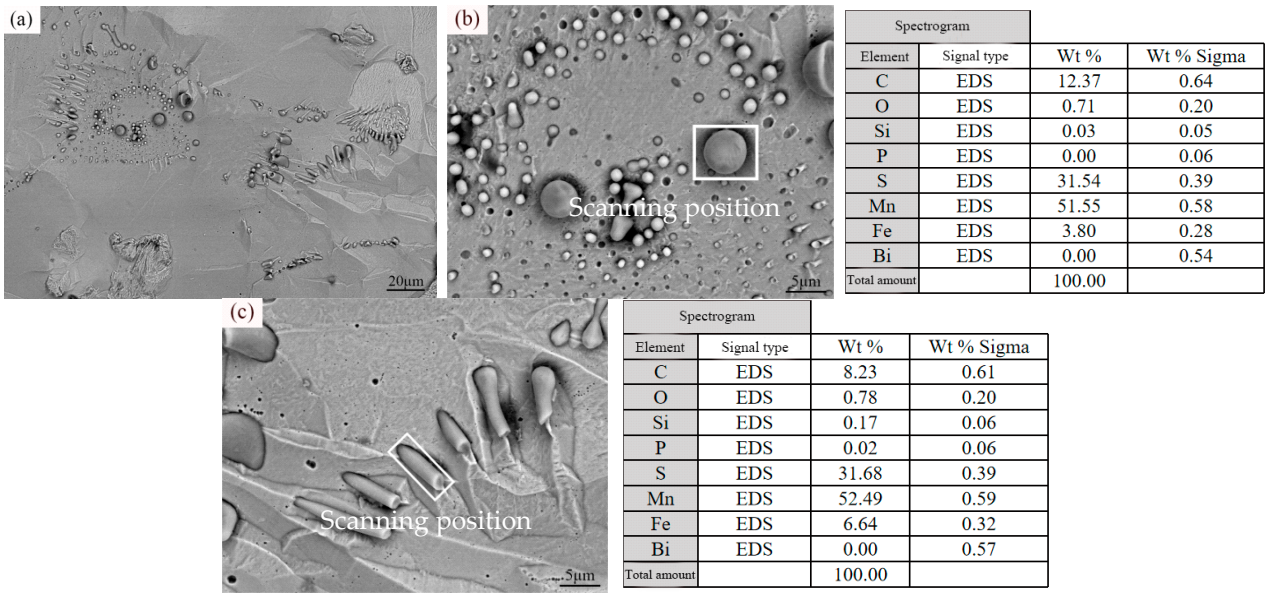
Figure 1. Microstructure of test steel: (**a**) 1#-0%-Bi; (**b**) 2#-0.010%-Bi; (**c**) 3#-0.013%-Bi; (**d**) 4#-0.022%-Bi; (**e**) 5#-0.026%-Bi; (**f**) 6#-0.031%-Bi.

3.2. Three-Dimensional Morphology Analysis of Nonmetallic Inclusions in Bismuth-Containing Free-Cutting Steel

The experimental steels (1) 1#, 0%-Bi, (2) 3#, 0.013%-Bi, (3) 5#, 0.026%-Bi, and (4) 6#, 0.031%-Bi with different bismuth contents were selected for 3D morphology observation.

3.2.1. Three-Dimensional Morphology of Nonmetallic Inclusions in Bismuth-Free Free-Cutting Steel

Figure 2 is the morphology inclusions captured by SEM + EDS after electrolysis of 1#. It can be seen from Figure 2a that the inclusions in 1# are mainly spherical and rod-shaped. Most of the spherical inclusions are about 1.5~2.5 μm in size, and the distribution is relatively clustered, and some of the larger spherical inclusions (4~7 μm) are distributed around the small-sized inclusions. The size of the rod and bar inclusions is mostly between 5 and 7 μm and distributed in a divergent way, and the largest rod and bar inclusions are 13.56 μm. The spherical and rod-like MnS inclusions are shown in Figure 2b,c, analyzed through point scanning.



Spectrogram			
Element	Signal type	Wt %	Wt % Sigma
C	EDS	12.37	0.64
O	EDS	0.71	0.20
Si	EDS	0.03	0.05
P	EDS	0.00	0.06
S	EDS	31.54	0.39
Mn	EDS	51.55	0.58
Fe	EDS	3.80	0.28
Bi	EDS	0.00	0.54
Total amount		100.00	

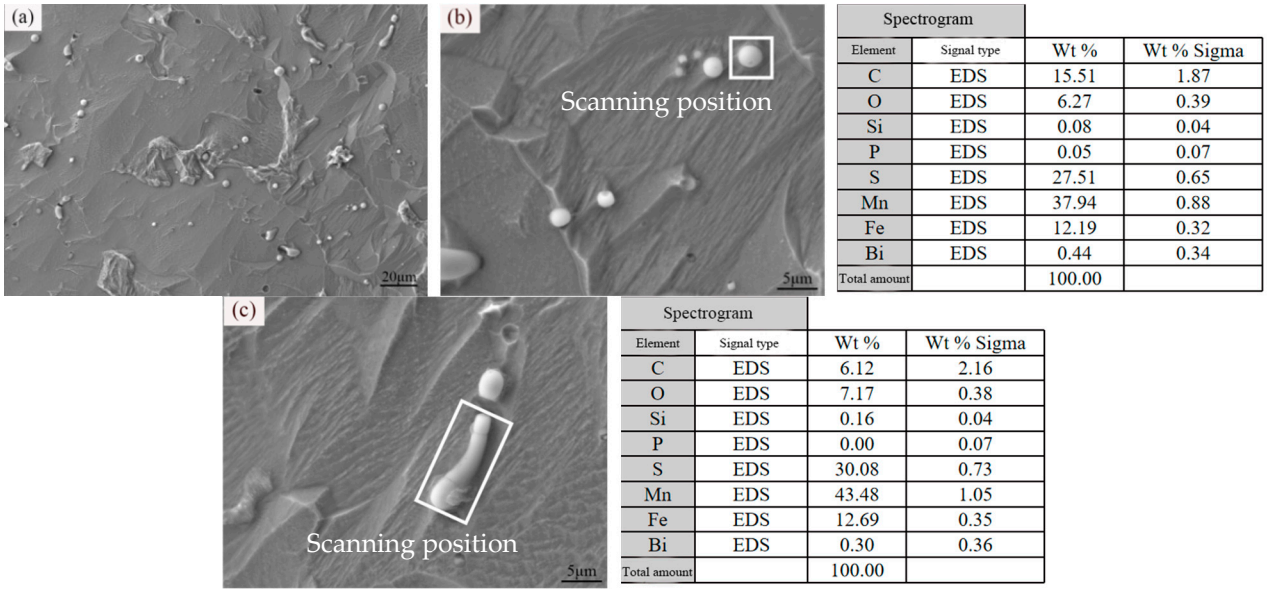
Spectrogram			
Element	Signal type	Wt %	Wt % Sigma
C	EDS	8.23	0.61
O	EDS	0.78	0.20
Si	EDS	0.17	0.06
P	EDS	0.02	0.06
S	EDS	31.68	0.39
Mn	EDS	52.49	0.59
Fe	EDS	6.64	0.32
Bi	EDS	0.00	0.57
Total amount		100.00	

Figure 2. Morphology of inclusions captured by SEM + EDS after electrolysis of 1#: (**a**) overall morphology of inclusions; (**b**) spherical MnS inclusions analyzed by point scanning; (**c**) rod-like MnS inclusions analyzed by point scanning.

3.2.2. Three-Dimensional Morphology of Nonmetallic Inclusions in Bismuth-Containing Free-Cutting Steel

Figure 3 shows the morphology inclusions captured by SEM after electrolysis of 3#. The inclusions of 3# are mostly spherical in shape, and some are rod-like, which are relatively evenly dispersed in the steel matrix, as shown in Figure 3a. The size of the spherical inclusions is basically between 2.5 and 5 μm, and the aspect ratio is close to 1. The length of the rod-like inclusions is mainly about 6.5~8.2 μm, and the largest rod-like inclusions have a size of 12.63 μm. Through point scanning analysis of the spherical and rod-like inclusions in the steel, it can be seen that the inclusions are MnS and that bismuth elements are attached to the MnS inclusions, as shown in Figure 3b,c.

The morphology of inclusions captured by SEM + EDS after electrolysis of 5# is shown in Figure 4. It can be found that there are spherical, rod-like, and fusiform inclusions in the test steel, and there are some small-sized white spherical substances in the matrix. The size of the spherical inclusions ranges from 5.15 μm to 6.67 μm, and the largest rod inclusion size is 14.41 μm. Through energy spectrum analysis, it is found that the composition of the inclusions is MnS, while the bright white phase in the inclusions and steel matrix is bismuth, as shown in Figure 4b,c.



Spectrogram			
Element	Signal type	Wt %	Wt % Sigma
C	EDS	15.51	1.87
O	EDS	6.27	0.39
Si	EDS	0.08	0.04
P	EDS	0.05	0.07
S	EDS	27.51	0.65
Mn	EDS	37.94	0.88
Fe	EDS	12.19	0.32
Bi	EDS	0.44	0.34
Total amount		100.00	

Spectrogram			
Element	Signal type	Wt %	Wt % Sigma
C	EDS	6.12	2.16
O	EDS	7.17	0.38
Si	EDS	0.16	0.04
P	EDS	0.00	0.07
S	EDS	30.08	0.73
Mn	EDS	43.48	1.05
Fe	EDS	12.69	0.35
Bi	EDS	0.30	0.36
Total amount		100.00	

Figure 3. Morphology of inclusions captured by SEM + EDS after electrolysis of 3# (Bi-0.013%): (**a**) overall morphology of inclusions; (**b**) spherical MnS inclusions analyzed by point scanning; (**c**) rod-like MnS inclusions analyzed by point scanning.

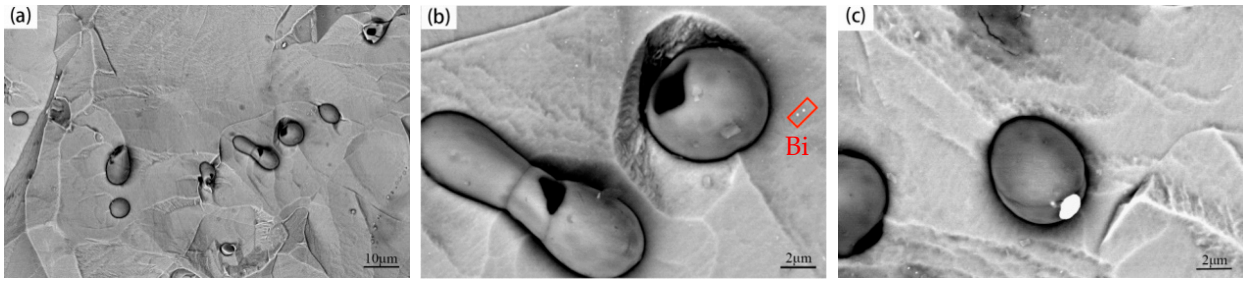


Figure 4. Morphology inclusions captured by SEM after electrolysis of 5# (Bi-0.026%): (**a**) overall morphology of inclusions; (**b**) Bi element in steel matrix; (**c**) Bi element in inclusions.

The morphology of inclusions captured by SEM + EDS after electrolysis of 6# is shown in Figure 5. It can be seen that the shape of the inclusions is mainly spherical and rod-shaped, and most of these inclusions are distributed unevenly at the grain boundaries in a chain shape or a divergent shape. The size of most of the rod-shaped inclusions is between 3.5 and 5.5 μm, the largest rod-shaped inclusion is 16.04 μm, and the aspect ratio reaches 5.4. Through line scanning analysis of the inclusions, it can be seen that the components of the inclusions are MnS, and the white material on the side of MnS inclusions is Bi, as shown in Figure 5b,c.

3.2.3. The Discussion of Bismuth Content on the Morphology and Distribution of MnS Inclusions

According to the above experimental phenomena, the addition of bismuth can affect the morphology, quantity, and distribution of MnS inclusions in free-cutting steel. The segregation of bismuth elements at the grain boundaries reduces the cohesion strength of the grain boundaries, resulting in a decrease in the combination of Mn and S particles at the grain boundaries. Therefore, the addition of bismuth reduces the number of MnS inclusions distributed at the grain boundaries. Meanwhile, the addition of bismuth can also lead to grain thinning and decrease grain boundary energy, so that the MnS inclusions will be spherical or elliptical.

The inclusions with different bismuth contents are different in shape, size, quantity, and distribution. The inclusions of 1# are large, and the size is small. The shapes of

the inclusions are spherical and rod-like, and most of them are clustered together along the grain boundaries. The inclusions of 3# are mainly spherical, which are most evenly distributed in the steel matrix, and the morphology and distribution of such kinds of inclusions are very favorable for the machinability of steel. According to the energy spectrum analysis of the free-cutting steel containing Bi, bismuth exists in two main forms; one is independently distributed in the steel matrix in the form of a single substance, and the other is dependent on MnS.

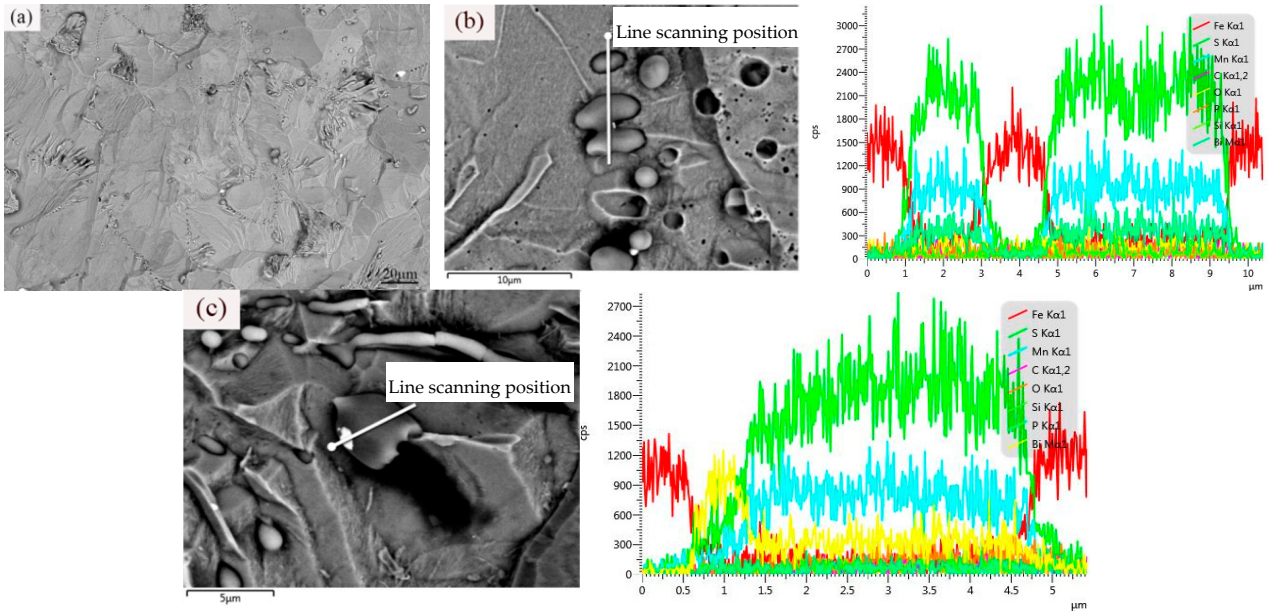


Figure 5. SEM + EDS diagram of inclusions after electrolysis of 6# (Bi-0.031%): (**a**) overall morphology of inclusions; (**b**) line scan of inclusions; (**c**) line scan of material on side of inclusions.

The addition of bismuth will affect the distribution and size of manganese sulfide inclusions in steel. When a certain amount of Bi is added from 0.010% to 0.020%, the inclusions distributed along the grain boundaries will decrease, while the large-sized inclusions will increase. If the added bismuth is excessive, the inclusions will gather at the grain boundaries. Therefore, it can be concluded that adding the appropriate content of bismuth can improve the morphology and distribution of inclusions and thus improve the cutting performance.

3.3. In Situ CSLM Observation of MnS Inclusions in Bismuth-Containing Free-Cutting Steel during Heating

3.3.1. Experimental Scheme

The sample steel with four different chemical compositions (1#, 2#, 3#, 4#, 6#) was heated at 5 °C/s to 1250 °C, and after holding for 180 s, it was cooled to room temperature at 2 °C/s, and the changes in the microstructure and inclusions of the sample steel were observed during the heating process.

The 4# steel sample was heated to 1250 °C at a rate of 1 °C/s, 5 °C/s, and 10 °C/s, and then cooled to room temperature at a cooling rate of 2 °C/s after 180 s of insulation. The changes in the microstructure and inclusions of the sample steel were observed during the heating process.

3.3.2. Influence of Bismuth Content on MnS Inclusions in Bismuth-Series Free-Cutting Steel

In order to investigate the effect of bismuth content on the microstructure and inclusions of bismuth-containing free-cutting steel, experimental steels 1# (without bismuth), 2# (Bi-0.010%), and 6# (Bi-0.031%) with different bismuth contents were selected for in situ observation at high temperatures, and their evolution process was analyzed.

Figure 6 shows the morphological evolution of the inclusions during the continuous heating process of 1#. It can be seen that the inclusions present a linear or divergent distribution at a normal temperature, with a small and dense size, and the inclusions are not obvious on the whole, as shown in Figure 6a. When the temperature rises to 547.2 °C, the grain boundaries of the ferrite structure can be clearly observed, and the inclusions gradually appear clearly, as shown in Figure 6b. As the temperature rises to 1003.7 °C, some small-sized inclusions have gradually disappeared, and the inclusions have a tendency to gradually join together, as shown in Figure 6c. When the temperature is up to 1250 °C, it can be seen that the inclusions are distributed along the austenite grain boundaries, some inclusions have been connected together, and the spheroidization phenomenon of larger inclusions is not obvious, as shown in Figure 6d.

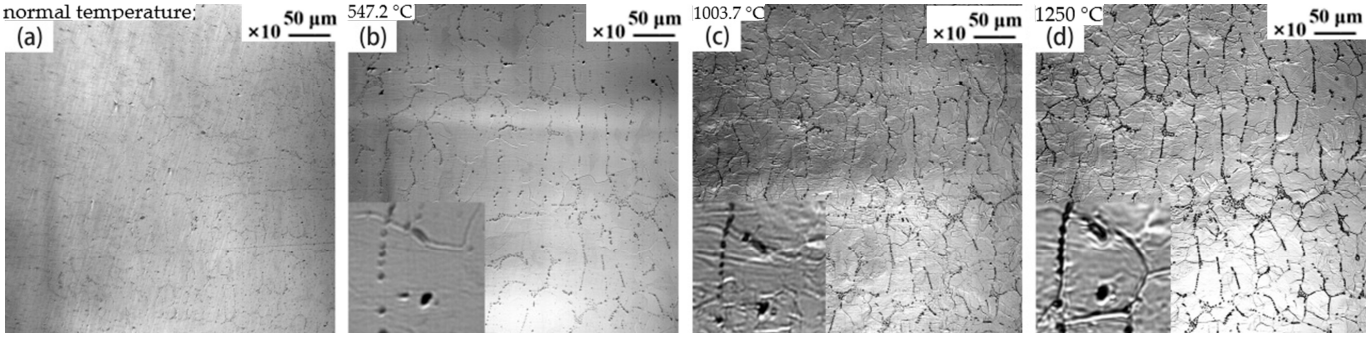


Figure 6. Morphological evolution of microstructure and inclusions of 1# (without bismuth) during heating: (**a**) normal temperature; (**b**) 547.2 °C; (**c**) 1003.7 °C; (**d**) 1250 °C.

Figure 7 shows the evolution of the microstructure and inclusions of 2# during the heating process. At a normal temperature, the inclusions of 2# are more evenly distributed in the steel matrix in the shape of lines, chains, or dots, as shown in Figure 7a. At 790 °C, ferritic grain boundaries can be clearly observed, and the volume of inclusions increases, as shown in Figure 7b. As the temperature increases to 1009 °C, some rod-like inclusions show a tendency to split, as shown in Figure 7c. At 1250 °C, the volume of inclusions increases, and spheroidization and fusification occur in some larger inclusions, as shown in Figure 7d.

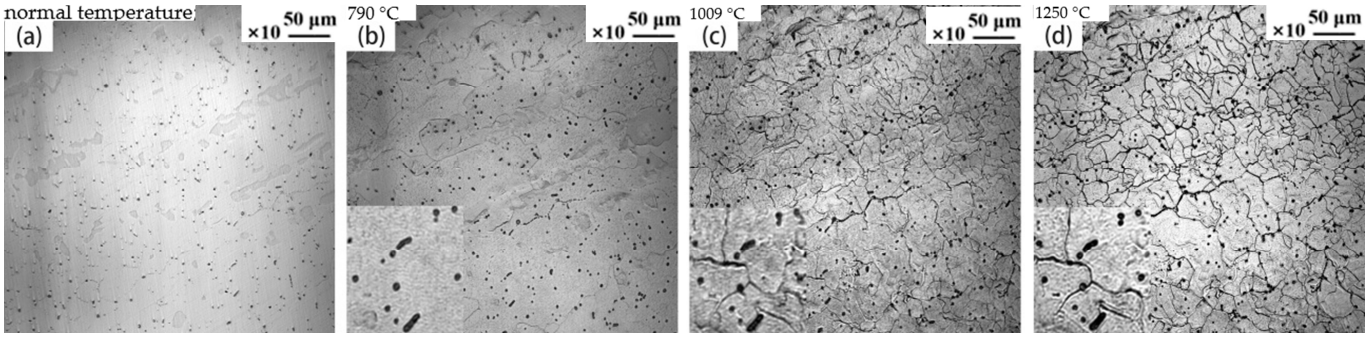


Figure 7. Morphological evolution of microstructure and inclusions of 2# (Bi-0.010%) during heating: (**a**) normal temperature; (**b**) 790 °C; (**c**) 1009 °C; (**d**) 1250 °C.

Figure 8 shows the evolution of the microstructure and inclusions of 6# steel during the heating process. At room temperature, the inclusions in 6# are mostly distributed along the grain boundaries in chains or clusters, and a few inclusions are dispersed with unclear profiles, as shown in Figure 8a. At 795.1 °C, the outer profile of the inclusions is very clear, and the grain boundaries are obvious at a low temperature, as shown in Figure 8b. During the subsequent heating process, the microstructure of the steel undergoes austenitic

transformation, and it is obvious that the inclusions are mainly clustered and distributed at the grain boundaries, while some inclusions also show spheroidization and passivation, as shown in Figure 8c,d.

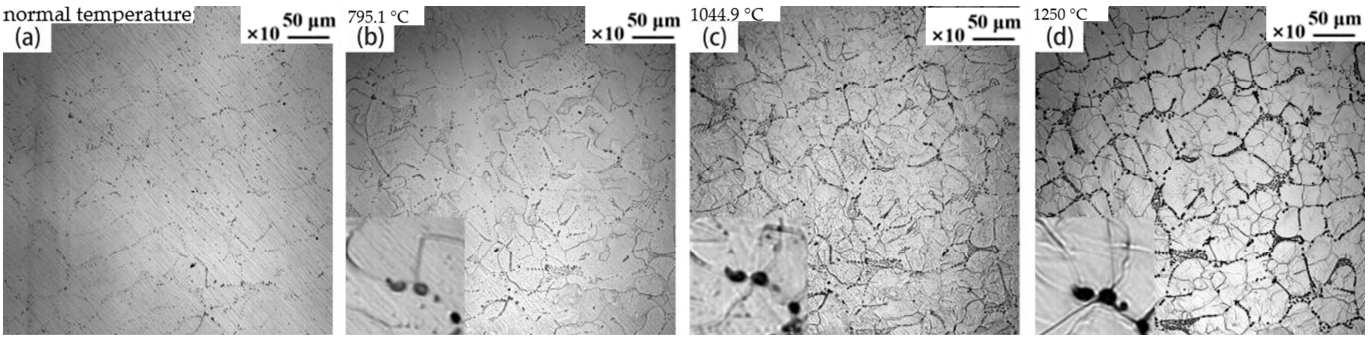


Figure 8. Morphological evolution of microstructure and inclusions of 6# (Bi-0.031%) during heating: (**a**) normal temperature; (**b**) 795.1 °C; (**c**) 1044.9 °C; (**d**) 1250 °C.

Through the analysis of the evolution of MnS inclusions during the heating process, it is found that the morphology of the inclusions in the non-bismuth free-cutting steel is not obvious, while the spheroidization and passivation of MnS inclusions are more and more obvious with the increase in the content of bismuth in the steel; therefore, the addition of Bi can promote the spheroidization of inclusions.

3.3.3. Influence of Heating Rate on MnS Inclusions in Bismuth-Series Free-Cutting Steel

Figure 9 shows the evolution process of MnS inclusions at different heating rates. It can be seen that when the heating rate is 1 °C/s, the size of MnS inclusions changes with the increase in temperature, as shown in Figure 9a. Spheroidization of short rod-like MnS inclusions occurs, and the longer rod-like sulfide even has a tendency to split. When the heating rate is increased to 5 °C/s and 10 °C/s, with the increase in temperature, the appearance of MnS inclusions does not change significantly and the number of MnS inclusions almost does not change, as shown in Figure 9b,c.

The above analysis shows that the transformation of rod-like and large-sized MnS inclusions into spherical or fusiform inclusions can be effectively controlled by reducing the heating rate, so as to obtain the ideal size and morphology of inclusions and thus improve the machining performance of bismuth-containing free-cutting steel.

3.3.4. Discussion of Evolution Mechanism of MnS Inclusions during Heating

Compared with non-bismuth free-cutting steel, the MnS inclusions of bismuth-containing free-cutting steel will spheroidize and passivate during heating. The reason for this phenomenon may be the lower melting point of bismuth and its insolubility in the steel matrix. During the heating process, bismuth will absorb part of the heat, at which time the energy of the MnS inclusions attached to bismuth will increase. In order to ensure that the manganese sulfide inclusions have the lowest Gibbs free energy to maintain their stable state, the manganese sulfide inclusions will spontaneously transform into spheroids with the lowest surface energy. During the heating process, the morphology of the MnS inclusions in bismuth-containing free-cutting steel changes, and its evolution behavior conforms to the Ostwald growth phenomenon.

$$\frac{dr_i}{dt} = \frac{2D\gamma\Omega^2 C_m}{RTr_1}\left(\frac{1}{r_2} - \frac{1}{r_1}\right) \quad (1)$$

where r_1 and r_2 are the radii of different manganese sulfide inclusions, D is a constant, γ is the specific interface energy, Ω is the molar volume, and C_m is the equilibrium solution concentration of manganese sulfide. According to Equation (1) [29], when $r_1 < r_2$, MnS gradually dissolves and becomes smaller. When $r_1 < r_2$, MnS grows larger and the inclusions

become larger in size. Therefore, with the increase in temperature and the extension of holding time, the small-sized inclusions of MnS gradually disappear in the heating process, while the larger-sized inclusions of MnS become larger and larger.

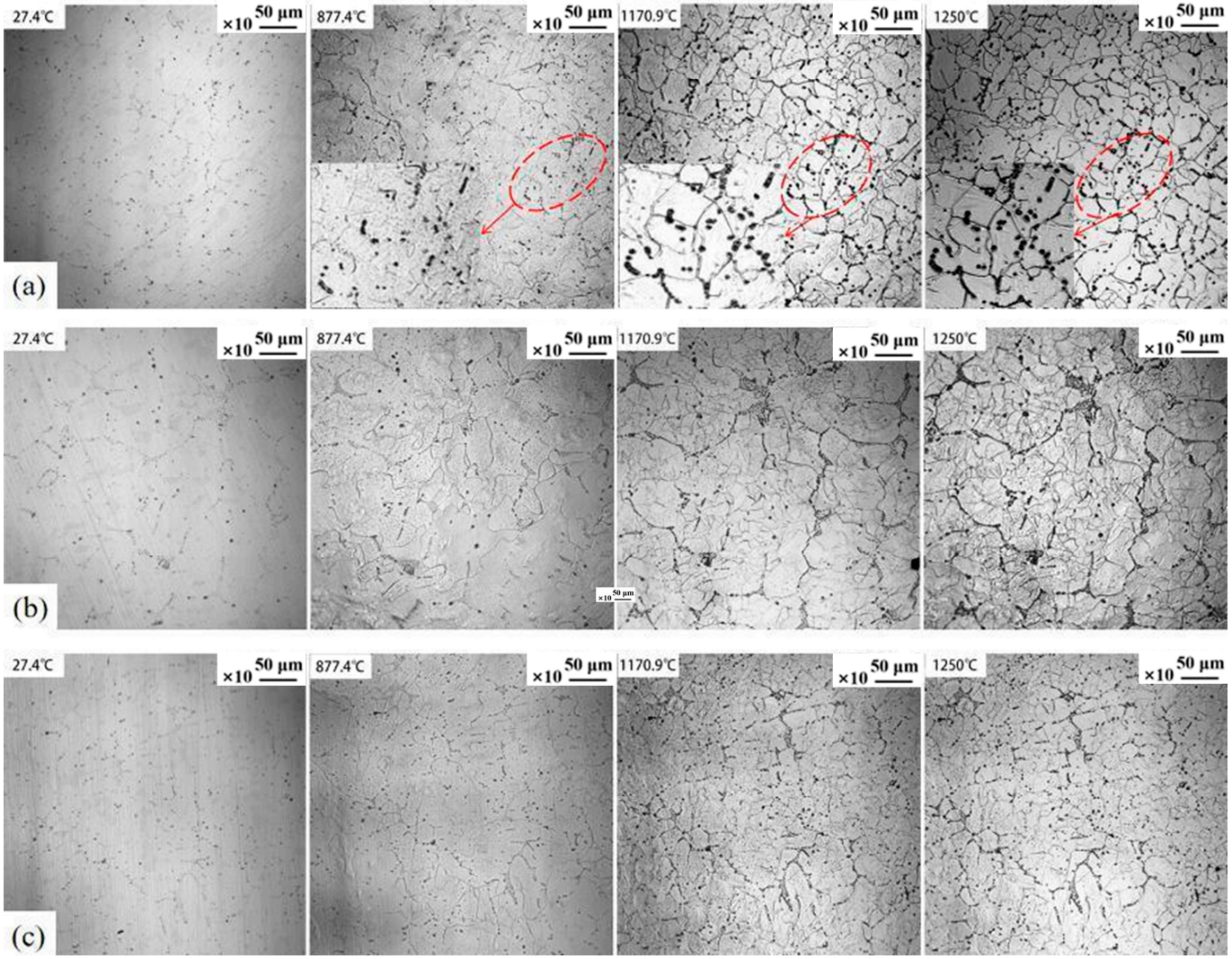


Figure 9. Morphological evolution of MnS inclusions at different heating rates: (**a**) 1 °C/s; (**b**) 5 °C/s; (**c**) 10 °C/s.

Nichols [30] found that the mechanism of inclusion evolution is due to the difference in surface curvature, resulting in different chemical potentials on the surface, which leads to the migration of Mn and S atoms, and finally causes the spheroidization or splitting of MnS.

The change in the morphology and size of the MnS inclusions in the bismuth-containing free-cutting process depends mainly on the diffusion of Mn or S elements between the matrix and the inclusions. For the growth of MnS particles in bismuth-containing free-cutting steel, the thermal energy of the elements increases with the increase in temperature, and the small-sized MnS particles are easier to diffuse until disappearing due to their small size. At this time, the concentration of Mn and S elements in the matrix increases, and the elements diffuse into the larger-sized MnS particles, thus making the larger-sized MnS particles increase. During the experiment, the slow heating rate and long holding time provide enough time for the diffusion of the elements and the accumulation of deformation energy, providing the possibility for nodulation of the inclusions.

4. Conclusions

OM and 3D electrolysis corrosion experiments were used to observe the microstructure of the experimental steel in its original state. It was found that there were spheroidal, rod-like, and irregularly shaped MnS inclusions in the bismuth-free free-cutting steel which were small in size and mostly distributed at the grain boundaries. When the right amount of bismuth is added to the free-cutting steel, the MnS inclusions are mainly spherical and spindle-shaped, and the distribution is relatively uniform and dispersed. There are two forms of bismuth in steel: one is the form of a single substance, distributed in the steel matrix, and the other is dependent on MnS.

The effects of the amount of bismuth and the heating rate on the evolution behavior of MnS inclusions in bismuth-containing free-cutting steel during heating were investigated through in situ observation experiments with a high-temperature confocal laser microscope. The results show that the addition of bismuth delayed the emergence of ferrite grain boundaries and helped spheroidize the MnS inclusions. A slower heating rate (1 °C/s) can make the Mn and S elements in the matrix fully diffuse, which provides the possibility for the spheroidization of the MnS inclusions.

According to the influence of the amount of bismuth on MnS precipitation in steel, it can be found that an appropriate amount of bismuth (0.022%) can promote the precipitation of MnS in the high-temperature region, and increasing the S content in the bismuth-containing free-cutting steel will also increase the precipitation amount of MnS.

Author Contributions: Investigation, writing—original draft, writing—review and editing, and methodology, C.X.; reviewing, investigating, and conceptualization, H.Z.; writing—review and editing, G.Z.; investigation, X.L.; reviewing, H.L. and G.Y.; reviewing and methodology, Z.J. All authors have read and agreed to the published version of the manuscript.

Funding: This study was funded by the National Natural Science Foundation of China (NSFC, No. 52274338) and a grant from the State Key Laboratory of Metal Material for Marine Equipment and Applications, grant numbers SKLMEA-K202211.

Data Availability Statement: The original contributions presented in the study are included in the article, further inquiries can be directed to the corresponding authors.

Conflicts of Interest: The authors declare no conflicts of interest.

References

1. Matsui, N.; Hasegawa, T.; Fujiwara, J. Effect of sulfide inclusion morphology on machinability and tool wear mechanism in low carbon free cutting steel. *J. Jpn. Soc. Precis. Eng.* **2011**, *77*, 322–326. [CrossRef]
2. Wang, Y.; Chen, X.; Zuo, P.P.; Wu, X.C. Influence of copper and sulfur on the cutting performance of P20-type plastic mold steel. *Met. Met. Matrix Compos.* **2022**, *36*, 173–179.
3. Kurka, V.; Kuboň, Z.; Kander, L.; Jonšta, P.; Kotásek, O. The effect of bismuth on technological and material characteristics of low-alloyed automotive steels with a good machinability. *Metals* **2022**, *12*, 301. [CrossRef]
4. Jia, Y.J.; Wang, F.M.; Wang, S.J.; Fan, D.D.; Li, J. Composition and microstructure analysis of domestic and foreign sulphur-containing free-cutting non-tempered steels. *Steelmaking* **2013**, *29*, 58–61. (In Chinese)
5. Liu, N.; Xie, J.; Shen, P.; Xu, X.; Fu, J. In-situ study of microstructures and sulphides and machinability of Bi-bearing free-cutting steels. *Ironmak. Steelmak.* **2023**, *50*, 310–320. [CrossRef]
6. VRyabov, A. Medium-carbon free-cutting steel. *Mater. Sci. Forum* **2019**, *946*, 47–52. [CrossRef]
7. Rečnik, S.; Vončina, M.; Nagode, A.; Medved, J. Thermodynamic and microstructural analysis of lead-free machining aluminium alloys with indium and bismuth additions. *Materials* **2023**, *16*, 6241. [CrossRef]
8. Liu, H.T.; Chen, W.Q. Research on recovery for adding low melting point metal bismuth to eco-friendly Bi–S based free cutting steel. *Ironmak. Steelmak.* **2014**, *41*, 355–359. [CrossRef]
9. Liu, H.; Chen, W.; Li, W.; Yu, Y. Solubility of bismuth in liquid Bi-S based free cutting steel. *High Temp. Mater. Process.* **2014**, *33*, 187–191. [CrossRef]
10. Toulfatzis, A.I.; Pantazopoulos, G.A.; David, C.N.; Sagris, D.S.; Paipetis, A.S. Machinability of eco-friendly lead-free brass alloys: Cutting-force and surface-roughness optimization. *Metals* **2018**, *8*, 250. [CrossRef]
11. Zhitenev, A.; Rovbo, A.; Nechaev, D.; Shaposhnikov, N.; Ryaboshuk, S.; Alkhimenko, A. Control of bismuth and manganese sulfide inclusions in free-cutting steels of different classes. *Metals* **2022**, *12*, 2076. [CrossRef]

12. Xu, X.; Chung, T.F.; Hu, S.; Zhu, Q.; Fu, J.; Yang, J.R.; Tian, Q. Effect of tin microalloying on the microstructure of low-carbon free-machining steels. *J. Mater. Res. Technol.* **2022**, *20*, 1172–1185. [CrossRef]
13. Masuda, K.; Ishihara, S.; Oguma, N.; Ishiguro, M.; Sakamoto, Y.; Iwasaki, M. Study on the fatigue crack initiation and growth behavior in bismuth-and lead-based free-cutting brasses. *Materials* **2022**, *15*, 7488. [CrossRef] [PubMed]
14. Yang, Y.; Zhan, D.; Qiu, G.; Li, X.; Jiang, Z.; Zhang, H. Inclusion evolution in solid steel during rolling deformation: A review. *J. Mater. Res. Technol.* **2022**, *18*, 5103–5115. [CrossRef]
15. Xu, X.Y.; Zeng, Z.Q.; Tian, Q.R.; Cao, C.W.; Shen, P.; Fu, J.X. Application of fractal theory to study morphology of manganese sulfide inclusion in resulfurized free-cutting steels. *J. Iron Steel Res. Int.* **2023**, *30*, 137–149. [CrossRef]
16. Shen, C.; Yang, Z.; Guo, J.B.; Lu, Q. Laboratory study on the precipitation of MnS in solid low-sulfur steel. *Steelmaking* **2022**, *38*, 49–55. (In Chinese)
17. Liu, W.; Yang, S.F.; Li, J. Research progress on motion behavior of nonmetallic inclusions at steel-slag interface. *Chin. J. Eng. Sci.* **2021**, *43*, 1647–1655. (In Chinese)
18. Shen, C.; Zheng, F.Z.; Chen, J.; Yang, Z. In-situ observation of Al_2O_3 inclusion formation and aggregation in steel. *Vanadium Titan. Steel* **2020**, *41*, 128–131+142. (In Chinese)
19. Shao, X.; Wang, X.C.; Jiang, M.; Wang, W.J.; Huang, F.X.; Ji, Y.Q. Dynamic in-situ observation of Mns inclusions behavior in sulfur series free-cutting steel during heating. *Acta Met. Sin.* **2011**, *47*, 1210–1215. (In Chinese)
20. Shao, X.J.; Wang, X.C.; Wang, W.J.; Huang, F.X.; Jiang, M. In-situ observation of the behavior of manganese sulfide inclusions in YF45MnV steel. *J. Univ. Sci. Technol. Beijing* **2010**, *32*, 570–573. (In Chinese)
21. Zhao, Y.; Li, T.; Tang, G.; Guo, H.; Yan, J.; Guo, X.; Zhu, Y. Characterization of the morphological evolution of MnS inclusions in free-cutting steel during heating. *Mater. Res. Technol.* **2022**, *17*, 1427–1437. [CrossRef]
22. Liu, J.Y.; Liu, C.S.; Bai, R.J.; Wang, W.; Wang, Q.B.; Zhang, H.; Ni, H.W. Morphological transformation of elongated MnS inclusions in non-quenched and tempered steel during isothermal heating. *J. Iron Steel Res. Int.* **2022**, *30*, 525–536. [CrossRef]
23. Hu, S.; Li, Z.; Fan, T.; Fu, J. Effect of bismuth on sulfide in high sulfur free-cutting steel. *Mater. Sci. Eng.* **2019**, *611*, 012017. [CrossRef]
24. Wang, X.; Zhang, H.; Wang, J.; Zhu, R.; Zhu, Y.; Lu, F.; Li, J.; Jiang, Z. Effect of bismuth and telluride on the inclusions of sulfur free-cutting steel. *Metals* **2023**, *13*, 486. [CrossRef]
25. Shen, P.; Zhang, D.; Zhang, H.; Ai, K.; Zhao, M.; Zeng, Z.; Fu, J. Study on the three-dimensional morphology of MnS inclusions in high sulphur steel. *Ironmak. Steelmak.* **2021**, *48*, 1179–1186. [CrossRef]
26. Xie, J.B.; Li, J.; Li, Z.W.; Wu, L.P.; Zhang, P.P.; Fu, J.X. Forms of Bi-sulphide in 1215MS steel related to machining and mechanical performance. *Ironmak. Steelmak.* **2021**, *48*, 927–935. [CrossRef]
27. Zhang, X.L.; Su, Y.Z.; Li, Y. Effect of matrix microstructure on machinability of low carbon and high sulfur free-cutting stee. *Met. Prod.* **2023**, *49*, 26–30. (In Chinese)
28. Che, Z.C.; Liu, W.; Yang, S.F. Effect of tellurium treatment on sulfide inclusion modification in 15–5PH steel. *Iron Steel* **2022**, *57*, 36–43. (In Chinese)
29. Yong, Q.L. Ostwald ripening of second phase particles in dilute solutions-I. Universal differential equations. *J. Iron Steel Res.* **1991**, *3*, 51–60. (In Chinese)
30. Nichols, F.A.; Mullins, W.W. Morphological changes of a surface of revolution due to capillarity-induced surface diffusion. *J. Appl. Phys.* **1965**, *36*, 1826–1835. [CrossRef]

Disclaimer/Publisher's Note: The statements, opinions and data contained in all publications are solely those of the individual author(s) and contributor(s) and not of MDPI and/or the editor(s). MDPI and/or the editor(s) disclaim responsibility for any injury to people or property resulting from any ideas, methods, instructions or products referred to in the content.